Structural Features of Paramyxovirus F Protein Required for Fusion Initiation†

Richard K. Plemper,‡ Ami S. Lakdawala,§ Kim M. Gernert,|| James P. Snyder,§ and Richard W. Compans*,‡

Department of Microbiology and Immunology, School of Medicine, 3001 Rollins Research Center, 1510 Clifton Road, Emory University, Atlanta, Georgia 30322, Department of Chemistry, 1515 Pierce Drive, Emory University, Atlanta, Georgia 30322, and BIMCORE (Molecular Graphics), G236 Rollins Research Center, 1510 Clifton Road, Emory University, Atlanta, Georgia 30322

Received March 7, 2003

ABSTRACT: On the basis of the coordinates of the related Newcastle disease virus (NDV) F protein, Valine-94, a determinant of measles virus (MV) cytopathicity, is predicted to lie in a cylindrical cavity with 10 Å diameter located at the F neck. A 16-residue domain around V94 is functionally interchangeable between NDV and MV F, supporting our homology model. Features of the cavity are conserved within the *Paramyxovirinae*. A hydrophobic base and a hydrophilic residue at the rim are required for surface expression. Small residue substitutions predicted to open the cavity were found to disrupt transport or limit fusogenicity of transport-competent mutants but can be compensated for by simultaneous insertion of larger residues at the opposing wall. Variants containing histidine substitutions mediate fusion at pH 8.5, while at pH 7.2 fusion is blocked, suggesting that functionality requires low charge in the cavity. These results indicate that specific structural features of the cavity are essential for paramyxovirus fusion initiation.

The Paramyxoviridae family of enveloped negative stranded RNA viruses encompasses a number of important human and animal pathogens including human and bovine respiratory syncytial virus, human parainfluenza viruses, Newcastle disease virus, mumps virus, and measles virus (*1*). Despite an efficient vaccine, MV[1] remains responsible for over 1 million deaths per year (*2*).

Paramyxovirus attachment to host cell receptors is mediated by the surface glycoprotein hemagglutinin (H), hemagglutinin-neuraminidase (HN), or glycoprotein (G), depending on the genus of virus (*3*). After receptor binding, in most cases these proteins provide fusion support for the fusion (F) glycoprotein, which is responsible for mediating virus-cell fusion in all Paramyxoviruses (*4*). F, a type I transmembrane glycoprotein, is synthesized as an inactive precursor F_0 that trimerizes in the endoplasmic reticulum (*5*, *6*) and is cleaved by furin in the late Golgi apparatus and trans-Golgi network to yield active complexes containing covalently linked F_1 and F_2 subunits (*7*, *8*). The newly generated N-terminus of F_1 possesses a hydrophobic stretch of amino acids termed the fusion peptide that is inserted into the target membrane during fusion.

Structural studies on a number of viral fusion proteins, particularly that of influenza virus, have suggested that prior to interaction with the host cell, fusion proteins exist in a metastable state. A trigger induces the conformational changes in the fusion protein required for exposure of the fusion peptide (*9*−*11*). While this trigger for influenza virus is the low pH of the endosome encountered by the virus following internalization, for the pH-independent Paramyxoviruses it is believed to be receptor binding (*4*). Crystallization of the NDV F protein revealed that the F protein trimer consists of a globular head held distal from the viral membrane by stalk and neck regions (*12*). Initial exposure of the fusion peptide has been suggested to rely on a shift or disassembly of the head region (*12*, *13*), conceivably mediated by a flexible domain that likely resides in the neck region.

Structures of fusion proteins, polypeptide fragments, or proteolytically stable cores in the final post-fusion state are available for fusion proteins of influenza (*14*), HIV (*15*, *16*), SIV (*17*), HTLV-1 (*18*), Moloney MLV (*19*), Ebola (*20*), RSV (*21*), SV5 (*22*), and NDV (*23*). All reveal a common six-helix coiled−coil bundle formed by three heterodimers of two heptad repeat regions (HR-A and HR-B), in which the fusion peptide and transmembrane domain, and thus the viral and cellular membranes, are brought into close proximity (*24*).

Besides this post-fusion structure, little information is available regarding the alterations that occur in the paramyxovirus F protein during fusion. The prefusion NDV structure gives no direct information regarding the mechanism of conformational changes in F. Furthermore, few analyses of the function of the F_2 subunit, an integral part of the F neck and head regions (*12*), in the fusion process have been reported since most studies have focused on the F_1 subunit that contains the fusion peptide and heptad repeats HR-A and -B. The NDV F crystal reveals a third heptad repeat region in the F neck, HR-C, that is located in F_2 immediately

† This work was supported by NIH grant CA18611 (to R.W.C.) and a Feodor Lynen fellowship from the Alexander von Humboldt foundation (to R.K.P.).

* Corresponding author. Phone: (404) 727-5947. Fax: (404) 727-5052. E-mail: compans@microbio.emory.edu.

‡ School of Medicine.

§ Department of Chemistry.

|| BIMCORE (Molecular Graphics).

[1] Abbreviations: MV, Measles virus; NDV, Newcastle disease virus; F protein, Fusion protein; H protein, hemagglutinin; HN, hemagglutinin-neuraminidase; G, glycoprotein; HR-A and -B, Heptad repeat A and B; MOI, multiplicity of infection; pfu, plaque forming units; $TCID_{50}$, median tissue culture infective dose.

10.1021/bi034385k CCC: $25.00
Published on Web 05/16/2003

N-terminal to the processing site (*12*) and is equivalent to the HR3 region recognized in RSV F (*25*, *26*). The N-terminal half of NDV F HR-C was suggested to pack in a parallel fashion into the groove of the HR-A coiled−coil. Downstream from a central proline residue that induces a kink in the helix, HR-C is thought to extend upward along the widening neck of the F protein (*12*).

Previously, we have shown by sequence alignment of NDV, SV5, and MV F proteins that SV5 and MV F_2 also possess potential HR-C domains (*27*). We demonstrated for MV F that the central proline in HR-C lies within an LXP motif conserved among these viruses and that its presence is essential for MV F protein folding. Furthermore, we found that amino acid 94, which lies in the putative outwardly kinked part of MV F HR-C, accounts solely for marked phenotypic differences observed between recombinant MV-Edm particles carrying the F protein of the Edmonston vaccine strain or the primary isolate MV-wtF. Our initial observations suggested that valine 94 may contribute to the initiation of membrane fusion.

In the current study, we have tested this hypothesis using a mutagenesis approach to dissect the role of residue 94 and neighboring amino acids in MV-induced fusion, based on modeling the structure of MV F protein using the X-ray data described for the NDV F protein. Having located valine 94 within a hydrophobic pocket at the top of the F neck region, we explored whether the physical dimensions and the biochemical properties of this region control the initiation of membrane fusion and hemifusion. Our findings suggest that the pocket is important for early F conformational changes necessary for fusion.

EXPERIMENTAL PROCEDURES

Cell Culture, Transfection, and Production of MV Stocks. Vero (African green monkey kidney) and HeLa cells were maintained in Dulbecco's modified Eagle's medium (DMEM) containing 10% fetal bovine serum (FBS), penicillin, and streptomycin at 37 °C and 5% CO_2. Stably transfected 293-3-46 helper cells (*28*) were grown in the presence of 1.2 μg/mL Geneticin. For transient transfection, Lipofectamine 2000 (Invitrogen) was used, and cells were analyzed 18−24 h post-transfection. To incubate cells at different pH conditions, CO_2 independent medium (Invitrogen) was adjusted to pH 8.5 and 7.2, respectively, and cells were maintained at 37 °C in the absence of additional CO_2.

To prepare virus stocks, Vero cells were infected at a multiplicity of infection (MOI) of 0.01 plaque forming units (pfu)/cell with the relevant virus and incubated at 37 °C. Cells were scraped in Opti-MEM (Invitrogen), and particles were released by three freeze−thaw cycles. Titers were determined by 50% tissue culture infective dose ($TCID_{50}$) titration on Vero cells according to the Spearmann−Karber method. Vaccinia virus titers were determined by plaque assays performed on HeLa cells.

Molecular Modeling of MV F. Sequence alignment was performed using the Clustal W algorithm (*29*). The sections of MV F not represented by structure in the NDV-F crystal (PDB code 1g5g) were not modeled. This includes residues 106−170 and the amino- and carboxy-termini, which were truncated at Asp33 and Gln454 in NDV F, respectively (*12*). Three-fold symmetry was achieved by including identical alignments between MV F and each monomer in the NDV F trimeric structure; no other manual restraints were added. MODELLER (*30*) was used to derive a list of spatial restraints for the trimer, generating the molecular probability density function (PDF) and to calculate a model optimizing the PDF by employing conjugate gradients and molecular dynamics. The resulting homology model was quality controlled by evaluating its Ramachandran plot and by applying the WHAT IF procedure (*31*). For both verification tools, the optimized homology model score was comparable to the NDV-F crystal structure. The resulting z-scores from the Ramachandran plot analysis, expressing how well the backbone conformations of all the protein residues correspond to known allowed regions, are similar but low, with −4.2 for the NDV-F crystal structure and −4.5 for the homology model. Structure assessment using WHAT IF gave good scores for normality of local amino acid environments, −0.9 for the NDV-F crystal structure and −1.2 for the model. These results indicate the model to be structurally equivalent to the crystal structure upon which it was templated and a reliable basis for further analysis and modeling. The SYBYL/Base package (Tripos Discovery Software, St. Louis, MO) was used for visualization and analysis of the structural model. For the generation of Connolly type surface models of 12.5 Å spheres around MV F residue V94, a dot density of 6 points/area and a probe radius of 1.4 Å were used.

Plasmid Construction. Parental plasmids for mutagenesis and all experiments were pCG-H and pCG-F encoding MV-Edm H and F (*32*) under the control of the CMV promoter. Site-directed mutagenesis was performed using the quick change system (Stratagene) and confirmed in all cases by DNA sequencing and Western analysis. Primer sequences are available upon request.

To transfer mutated F variants into a DNA copy of the MV genome, *Nar*I *Pac*I fragments of pCG-F containing the F open reading frame were cloned into *Nar*I *Pac*I digested p(+)MV-NSe (*33*), adhering to the reported rule of six (*34*).

Cell Fusion Assays. Vero cells (5×10^5) were cotransfected with 1.5 μg plasmid DNA each encoding MV-H and F using Lipofectamine 2000 (Invitrogen) and monitored 18 h post-transfection for syncytium formation using phase-contrast microscopy. Photographic documentation was performed at a magnification of 200×.

For quantification of fusion activity, Vero cells (5×10^5) were cotransfected with 1.5 μg of plasmid DNA each encoding MV-H and F and 3 μg of plasmid DNA encoding the β-galactosidase reporter gene under the control of the T7-promoter and incubated in the presence of 200 μM FIP. Twelve hours post-transfection 1.5×10^5 cells were washed in PBS and mixed with 3.0×10^5 cells of a population previously infected with vaccinia virus encoding T7 polymerase at an MOI of 3 pfu/cell. After incubation in 10% DMEM at 37 °C for 6 h, cells were lysed, and the β-galactosidase activity was assessed using the β-galactosidase assay kit (Invitrogen) according to the manufacturer's instructions. To quantify fusion activity at different pH conditions, after mixing of the two populations, cells were maintained in CO_2 independent medium adjusted to pH 8.5 or 7.2 as indicated in the absence of additional CO_2. As a minimum for all constructs, fusion activity was quantified in two independent experiments.

Recovery of Recombinant Viruses. Recombinant MV were generated essentially as described (*28*). Briefly, the helper cell line 293-3-46 stably expressing MV N, MV P, and T7 polymerase was transfected by calcium phosphate precipitation using the ProFection kit (Promega) with a DNA copy of the relevant MV genome and MV polymerase L. Helper cells were overlaid on Vero cells 76 h post-transfection, and resulting infectious centers were passaged on Vero cells.

RT-PCR. The integrity of recombinant MV particles was confirmed by reverse transcription PCR (RT-PCR) and DNA sequencing of the modified genes. After infection of Vero cells with independently recovered recombinant MV clones, total RNA was isolated for each clone using the RNeasy Mini Kit (Qiagen) and subjected to reverse transcription using Superscript II Reverse Transcriptase (Invitrogen) and random hexamer primers. Genome fragments containing the F gene were then amplified using the Expand High Fidelity PCR system (Roche) followed by sequencing of purified PCR products.

Virus Growth Kinetics. Vero cells (5×10^5 per time point) were infected with an MOI of 0.03 pfu/cell. At the indicated time points, cells were scraped in Opti-MEM (Invitrogen) and subjected to three freeze−thaw cycles, and cell associated titers were determined by $TCID_{50}$ titration on Vero cells according to the Spearmann−Karber method.

Western Analysis. Cells (5×10^5) were transfected with 2 μg of plasmid DNA encoding MV F constructs using Lipofectamine 2000. For infection, cells were infected with a MOI of 0.1 pfu/cell. Twenty hours post-transfection or 36 h post-infection, cells were washed in phosphate buffered saline (PBS), lysed for 10 min at 4 °C in lysis buffer (50 mM Tris, pH 8.0; 62.5 mM EDTA; 0.4% deoxycholate; 1% Igepal (Sigma)) containing protease inhibitors (Complete mix (Roche)) and 1 mM phenylmethylsulfonylfluoride (PMSF), and centrifuged at 5000*g* for 10 min at 4 °C. Total protein concentration of post-nuclear supernatants was determined using the DC Protein-Assay Kit (BioRad), and 2.5 μg of total protein was mixed with urea buffer (200 mM Tris, pH 6.8; 8 M urea; 5% sodium dodecyl sulfate (SDS); 0.1 mM EDTA; 0.03% bromphenolblue; 1.5% dithiothreitol) for 25 min at 50 °C. Samples were fractionated on SDS−polyacrylamide gels, blotted to poly(vinylidene difluoride) membranes (Millipore) and subjected to enhanced chemiluminescence detection (Amersham Pharmacia Biotech) using antibodies specific for the cytosolic tail of F (*35*).

Surface Biotinylation. Cells were transfected with 2 μg of plasmid DNA encoding MV F variants as indicated using Lipofectamine 2000. For infection, cells were infected with a MOI of 0.1 pfu/cell and analyzed 36 h post-infection. After washing in cold PBS, cells were incubated in PBS with 0.5 mg/mL NHS-SS-Biotin (Pierce) for 20 min at 4 °C followed by washing and quenching for 5 min at 4 °C in DMEM. Cells were scraped in immunoprecipitation buffer (10 mM Hepes, pH 7.4; 50 mM sodium pyrophosphate; 50 mM sodium fluoride; 50 mM sodium chloride; 5 mM EDTA; 5 mM EGTA; 100 mM sodium vanadate; 1% Triton X-100) containing protease inhibitors (Complete mix) and 1 mM PMSF, and lysates were cleared by centrifugation for 20 min at 20 000*g* and 4 °C. Biotinylated proteins were absorbed to Sepharose-coupled Streptavidin (Amersham Pharmacia Biotech) for 90 min at 4 °C, washed in buffer 1 (100 mM Tris, pH 7.6; 500 mM lithium chloride; 0.1% Triton X-100) then buffer 2 (20 mM Hepes, pH 7.2; 2 mM EGTA; 10 mM magnesium chloride; 0.1% Triton X-100), incubated in urea buffer for 25 min at 50 °C, and subjected to Western analysis using antibodies specific for the MV-F tail. For statistical analysis, Western blots were scanned to yield arbitrary densitometric units. Results were normalized to the control cells in each experiment.

Hemifusion Assay. Vero cells were cotransfected with 3 μg each of plasmid DNA encoding MV H and F variants as indicated and incubated in the presence of 200 μM fusion inhibitory peptide (FIP) (Bachem). Sixteen hours post-transfection, cells were washed repeatedly in PBS and overlaid with washed and Rhodamine18 (R18) (Molecular Probes)-labeled African green monkey-derived erythrocytes (Bio Whittaker). After binding of labeled erythrocytes for 1 h at 4 °C, cells were washed extensively in PBS and incubated at 37 °C for 30 min, and red fluorescence of Vero cells indicating dye transfer was assessed microscopically. Photographic documentation of fluorescence was performed at a magnification of 400×.

RESULTS

Modeling the Structure of MV F. To investigate the structural basis for the phenotypic differences determined by amino acid 94, we have applied computer-assisted molecular modeling to construct a homology model of the structure of the MV F protein on the basis of the X-ray coordinates reported for NDV F (*12*) (Brookhaven Protein Data Bank access code 1g5g), a paramyxovirus related to MV. The model is based on sequence alignment of F proteins derived from strains MV-Edmonston-tag and NDV-B1-Hitchner/47 (*27*) using Clustal W. Overall, both proteins share 27% amino acid identity and 48% similarity. Importantly, with the exception of some minor modifications at the immediate amino terminus, cysteine residues within the F ectodomain were completely conserved suggesting a similar structural framework based on the formation of intramolecular disulfide bridges (*27*, *36*). We used the MODELLER package (*30*) to generate a comparative protein structure for the MV F trimer by satisfaction of spatial restraints based on the NDV F trimer crystal structure (1g5g).

Localization of Residue V94 in the MV F Structure Model. The resulting model predicts a helical HR-C domain in MV F_2 containing a central proline residue in an L/IXP motif (*27*) that induces an outward kink in the helix, as does its homologue in NDV F (*12*). We localized valine 94, the residue that solely determines phenotypic differences between F-Edm and F-wtF (*27*), within this domain. This residue was predicted to be localized at the inner face of HR-C, pointing toward the center of the F trimer. When we identified side chains within a 5 Å distance and hence most likely in direct contact with V94, residue P224 was predicted to be present in the F_1 domain of the same and residues L256 and L257 in F_1 domains of an adjacent F monomer (Figure 1A). Both leucine residues are located in a short α-helical stretch of F_1 that runs across the HR-C helix so that L256 and L257 lie on either side of V94 (Figure 1A). Together, these residues are located on an internal surface at the top of the F neck region, immediately below the globular head (Figure 1B). When we obtained a Connolly type surface model of a 12.5 Å area around residue 94, we found that these residues are

FIGURE 1: Residue V94 lies within a defined cavity in the MV F structural model. (A) Predicted orientation of residues within 5 Å of V94. Backbones are shown as shaded ribbons colored by monomer yellow and cyan. Side chains of residues within 5 Å of V94 are represented as ball-and-stick models including van der Waals radii. (B) Location of the F cavity within the F trimer. Backbones are shown as shaded ribbons colored by monomer yellow, cyan, and orange, respectively, and residues within 5 Å of V94 are shown. (C) Connolly type surface model of the F cavity region, covering 15 Å around V94.

part of a cavity that resembles a rough cylinder with a diameter and a height of approximately 10 Å (Figure 1C). The walls and base of the cylinder are largely hydrophobic, containing the residues described above and four additional amino acids located in the F_1 domain of the same monomer as V94 but outside the 5 Å radius. The upper rim of the cavity is formed on one side by V94 and L257 and on the other by the hydrophilic residues R268 and T270. R268 contains the only charged side chain in this microdomain. Residues I269 and P224 constitute the lower walls and base of the cavity and I225 the back wall. Within a 5 Å distance of residue V94, L256 is oriented away from the plane of the surface and hence is not visible in the Connolly type model. In our homology model, the top of the described cavity is open to solvent, although during the conformational modifications that accompany fusion, it might be partially occluded.

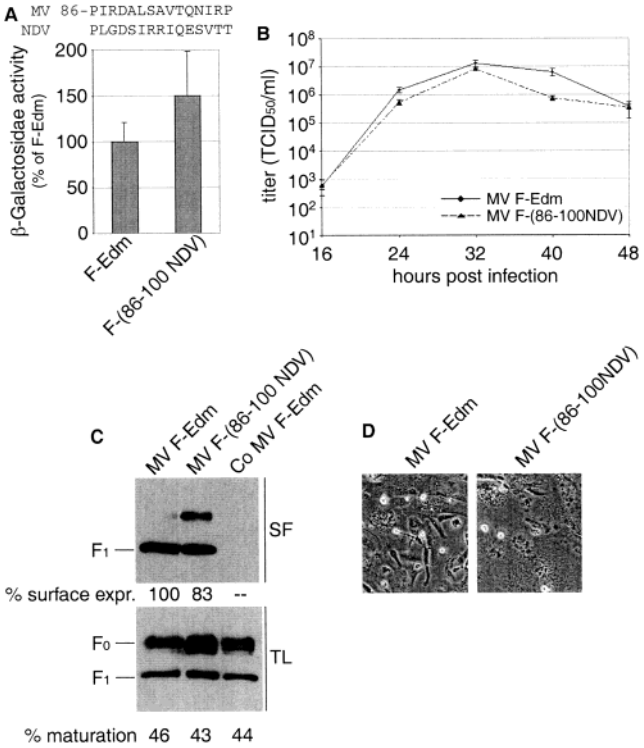

FIGURE 2: C-terminal half of NDV F HR-C is functionally interchangeable with that of MV. (A) Chimeric MV F protein carrying amino acids 86−100 of NDV F as depicted induces fusion at least as efficiently as F-Edm. Quantification of fusion activity of MV F variants coexpressed with MV-H. The relative percentage of β-galactosidase activity in relation to the activity induced by F-Edm is given. Recombinant MV F (86−100 NDV) carrying this chimeric F; (B) grows as efficiently; (C) shows a similar maturation rate and expresses similar cell-surface levels of F; and (D) induces extensive syncytium formation. For growth curves, Vero cells were infected with an MOI of 0.03 pfu/cell, and the titers of cell associated particles were determined by $TCID_{50}$ titration. Biotinylated F protein displayed at the cell surface (SF) and total cell lysate (TL) were detected by Western analysis using antibodies directed against the F cytosolic tail. For control (Co MV F-Edm), biotinylation of infected cells was omitted. Numbers indicate the relative percentage of F_1 detected in surface biotinylation in relation to F-Edm F_1 (% surface expression), and the relative percentage of the F_1 fraction in relation to the total F protein (% maturation). Biotinylation and photographic evaluation of syncytium formation was carried out 36 h after infection of Vero cells with an MOI of 0.1 pfu/cell. For syncytium formation, representative fields of view are shown.

The hydrophobicity distribution of the cavity (i.e., hydrophobic residues buried in its cleft and hydrophilic residues around the lower rim) is consistent with the thermodynamic tendency of hydrophobic residues to bury within the molecule (*37*, *38*).

NDV/MV Domain Swapping of the HR-C C-Terminal Half Supports the MV F Structural Model. If the structural prediction were correct that MV F_2 contains a helical HR-C domain as described for NDV F_2 (*12*), one would expect a functional analogy between the MV and the NDV HR-C regions. Thus, it might be possible to exchange the C-terminal outwardly kinked part of MV F HR-C with that of NDV F, despite its almost complete lack of sequence identity (Figure 2A); the N-terminal part of HR-C is suggested to pack into the HR-A domain and thus would not be expected

to be interchangeable (*12*). To assess the validity of the modeling approach for this region, we replaced the C-terminal half of the MV-Edm F HR-C domain with the homologous NDV sequence. A chimeric MV F molecule containing amino acids 86−100 of NDV F_2 instead of the corresponding region of MV F_2 was highly fusogenic in a quantitative assay when coexpressed with MV-H (Figure 2A). When this chimeric construct was transferred into a cDNA copy of the MV genome and recombinant virions containing MV-F (86−100 NDV) instead of MV-F were recovered, these particles grew with similar kinetics and to identical titers as the parental MV-Edm virus (Figure 2B). Furthermore, surface biotinylation of cells infected with MV-F (86−100 NDV) revealed that the surface steady-state levels of the chimeric F_1 protein were similar to those of MV-Edm F_1 (Figure 2C), although we detected some uncleaved MV-F_0 (86−100 NDV) moieties at the surface suggesting a slight reduction in the efficiency of their proteolytic processing. Since the fusion activity of the recombinant virus was at least as efficient as that of MV-Edm (Figure 2D), we concluded that these MV and NDV HR-C regions are functionally interchangeable, supporting the model prediction that this region is also helical in MV F protein.

Mutational Analysis of the F Pocket. In previous studies, we observed that substitutions to smaller amino acids, alanine and glycine, were well-tolerated at position 94, while changes to charged or polar residues interfered either with F processing or fusion and hemifusion activity (*27*). To assess the individual role of all residues in the potential cavity for F folding and fusion activity, we undertook a mutational analysis of this region (summarized in Table 1). Following transient expression, all mutants were analyzed for their steady-state expression level (not shown) and degree of cell surface expression. Fusion activity was assessed microscopically and by using a β-galactosidase reporter gene-based quantitative fusion assay. Some mutants with very low surface expression levels were found to induce syncytium formation albeit to a lower degree (Table 1, nos. 10, 52, and 53). For this reason, hemifusion capacity was also determined for all mutants that induced no visible syncytium formation and reached less than 15% of F-Edm-mediated β-galactosidase activity in the quantitative fusion assay. Neither of these mutants was able to mediate hemifusion (Table 1) suggesting that functionality of the F cavity is required for initial steps of the fusion process.

Figure 3A summarizes the results of our mutagenesis for all residues in a color-coded Connolly type surface model that denotes how sensitive each position is to change. All residues were primarily assessed for their sensitivity to substitution with alanine. For most positions, however, additional mutations were generated and also considered for the model. These MV-F based results were corroborated by a sequence alignment of representative viruses of each genus of the subfamily *Paramyxovirinae* (Figure 3B). The properties of residues least tolerant to substitutions, R268 and I269 in MV numbering, are most highly conserved among members of different *Paramyxovirinae*, while for the most tolerant residue, L257, no consensus sequence could be calculated. In the following text, selected sets of mutants with distinct phenotypes will be discussed in detail.

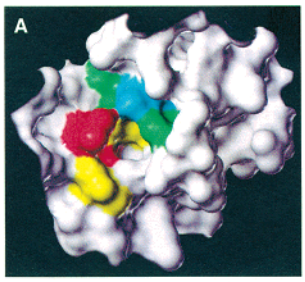

B

NDV B1-H./47	102-I...	228-PA...	260-LS...	272-NPI...
SV5 W3	90-I...	214-PA...	246-AA...	258-QIV...
Mumps RW	90-I...	214-PA...	246-AA...	258-QIV...
HPIV4a	91-L...	215-PA...	247-AA...	259-QII...
Measles	94-V...	224-PI...	256-LL...	268-RIT...
CDV	206-M...	336-PI...	368-MI...	380-KIT...
Nipah	97-Y...	221-PV...	253-FD...	265-QII...
Hendra	97-Y...	221-PV...	253-FD...	265-QIV...
HPIV1	96-Q...	228-IG...	260-IY...	272-TVI...
HPIV3	89-Q...	221-LQ...	253-IY...	265-RVI...
Consensus	I	PA	I	QII

FIGURE 3: Tolerability to change of residues within the F pocket correlates with their degree of conservation among the Paramyxovirinae. (A) Color-coded Connolly type surface model of tolerance of residues within the pocket to mutagenesis based on single alanine substitutions shown in Table 1. Residues colored red are most sensitive to substitutions, followed by yellow and green, while blue denotes side chains that are most tolerant to alterations. (B) Alignment of F sequences from representative viruses of all Paramyxovirinae genera, showing amino acids within the pocket. The consensus sequence as calculated by Clustal W is given. Residues identical in several viruses are marked in blue, and residues with similar biophysical properties are indicated in green.

Biophysical Properties of the Pocket. To probe the necessity for hydrophobic residues at the base of the cavity, we changed P224 to a smaller, less hydrophobic alanine residue. Mutating P224 reduced F processing to 15% of F-Edm levels, yet only reduced fusogenicity to 87% (Table 1, no. 10). Mutating I269 at the base of the cavity to alanine (Table 1, no. 22) or histidine (Table 1, no. 24) completely ablated F proteolytic processing and cell surface expression, thus also ablating fusogenicity (Figure 4A−C). In contrast, replacing hydrophobic I269 with a hydrophobic valine (Table 1, no. 23) resulted in an F mutant that was processed and efficiently surface expressed and was able to induce extensive cell-to-cell fusion (Figure 4A−C). These findings suggest that hydrophobic residues at the base of the cavity are required for proper F folding, implicating hydrophobicity as a driving force for formation of the F pocket. Importantly, hydrophobicity of residues corresponding to MV I269 is conserved among *Paramyxovirinae* F proteins (Figure 3B).

The polar character of the arginine residue at the hydrophilic rim of the MV F pocket is also mostly conserved in *Paramyxovirinae* F proteins (asparagine in NDV and glutamine in SV5, respectively). Substituting a nonpolar alanine residue for R268 disrupted F processing and surface expression (Table 1, no. 20), while introducing a basic histidine residue, which is not present at this position in any analyzed *Paramyxovirinae* family member, reduced surface expression to 50% but did not affect fusion activity (Table 1, no. 21).

Small Amino Acid Substitutions in the Pocket Can Be Compensated for by Larger Residues at the Opposing Side. To analyze the physical properties of the cavity predicted by the structural model, we hypothesized that widening of

Table 1: Summary of Mutations Made in Residues of the MV F Pocket[a]

		genotype								phenotype			
	No	AA 94	AA 224	AA 225	AA 256	AA 257	AA 268	AA 269	AA 270	Surface Expr. (% of F-Edm)	β-Gal activity (% of F-Edm)	Lipid mixing	β-Gal activity (% of F-Edm, pH 8.5)
F-Edm	1 (27)	V	P	I	L	L	R	I	T	100	100 (11)	yes	100 (21)
single mutations	2 (27)	**M**	P	I	L	L	R	I	T	100	43 (31)	yes	
	3 (27)	**A**	P	I	L	L	R	I	T	85	107 (11)	yes	
	4 (27)	**G**	P	I	L	L	R	I	T	35	60 (5)	yes	
	5	**H**	P	I	L	L	R	I	T	55	48 (10)		
	6 (27)	**N**	P	I	L	L	R	I	T	60	3 (3)	no	
	7 (27)	**E**	P	I	L	L	R	I	T	<5	1 (7)	no	
	8	**C**	P	I	L	L	R	I	T	60	119 (18)		
	9	**Y**	P	I	L	L	R	I	T	105	96 (29)		
	10	V	**A**	I	L	L	R	I	T	15	87 (25)		
	11	V	P	**A**	L	L	R	I	T	100	82 (32)		
	12	V	P	I	**A**	L	R	I	T	90	74 (11)	yes	
	13	V	P	I	**H**	L	R	I	T	90	92 (3)		
	14	V	P	I	**D**	L	R	I	T	5	13 (23)	no	
	15	V	P	I	L	**A**	R	I	T	120	97 (33)		
	16	V	P	I	L	**C**	R	I	T	55	118 (1)		
	17	V	P	I	L	**K**	R	I	T	105	96 (6)		
	18	V	P	I	L	**D**	R	I	T	65	65 (52)	yes	
	19	V	P	I	L	**H**	R	I	T	95	86 (61)		
	20	V	P	I	L	L	**A**	I	T	<5	12 (3)	no	
	21	V	P	I	L	L	**H**	I	T	50	92 (30)		
	22	V	P	I	L	L	R	**A**	T	<5	1 (11)	no	
	23	V	P	I	L	L	R	**V**	T	50	97 (55)		
	24	V	P	I	L	L	R	**H**	T	<5	0 (2)	no	
	25	V	P	I	L	L	R	I	**A**	100	55 (24)		
	26	V	P	I	L	L	R	I	**H**	30	1 (4)	no (pH 7.2)	28 (2)
	27	V	P	I	L	L	R	I	**S**	100	93 (7)		
double mutations	28	**M**	**A**	I	L	L	R	I	T	80	49 (11)		
	29	**A**	**A**	I	L	L	R	I	T	25	60 (34)	yes	
	30	**G**	**A**	I	L	L	R	I	T	<5	1 (2)	no	
	31	**M**	P	**A**	L	L	R	I	T	100	111 (15)		
	32	**A**	P	**A**	L	L	R	I	T	90	81 (20)		
	33	**G**	P	**A**	L	L	R	I	T	25	0 (3)	no	
	34	**M**	P	I	**A**	L	R	I	T	100	94 (14)		
	35	**A**	P	I	**A**	L	R	I	T	20	38 (8)		
	36	**G**	P	I	**A**	L	R	I	T	<5	6 (7)	no	
	37	**N**	P	I	**D**	L	R	I	T	<5	1 (5)	no	
	38	**A**	P	I	L	**A**	R	I	T	100	65 (18)		
	39	**A**	P	I	L	**K**	R	I	T	75	96 (7)		
	40	**G**	P	I	L	**A**	R	I	T	50	11 (22)	no	
	41	**N**	P	I	L	**D**	R	I	T	<5	1 (6)	no	
	42	**H**	P	I	L	L	R	I	**H**	12	14 (1)	no (pH 7.2)	52 (6)
	43	V	**A**	**A**	L	L	R	I	T	25	71 (52)	yes	
	44	V	P	I	**A**	**A**	R	I	T	30	56 (8)		
	45	V	P	I	L	**H**	R	I	**H**	50	48 (4)	no (pH 7.2)	80 (1)
multiple mutations	46	**M**	**A**	**A**	L	L	R	I	T	35	60 (10)		
	47	**A**	**A**	**A**	L	L	R	I	T	10	19 (9)	yes	
	48	**M**	P	I	**A**	**A**	R	I	T	105	105 (12)		
	49	**A**	P	I	**A**	**A**	R	I	T	5	7 (15)	no	
	50	V	**A**	I	**A**	**A**	R	I	T	<5	11 (2)	no	
	51	V	P	**A**	**A**	**A**	R	I	T	65	19 (22)	no	
	52	**M**	**A**	I	**A**	**A**	R	I	T	5	32 (18)		
	53	**M**	P	**A**	**A**	**A**	R	I	T	5	33 (15)		
	54	**M**	**A**	**A**	**A**	**A**	R	I	T	<5	13 (2)	no	

[a] All mutant proteins were assessed for their cell surface expression by surface biotinylation, ability to induce syncytium formation, and ability to induce hemifusion where indicated. Percentages are rounded to the nearest 5. Shaded boxes indicate no visible syncytium formation.

its central cleft through substitution with smaller side chains while maintaining hydrophobicity at its base should result in loss of fusion activity either because of impaired folding and hence reduced F surface expression or specific loss of function of surface exposed F molecules. One would predict, however, that loss of function because of the introduction of smaller residues in the pocket might be compensated for by simultaneous insertion of larger residues at opposing positions.

We therefore mutated amino acids L256 and L257 to smaller alanine residues (Table 1, no. 44). L256 lies within a 5 Å distance of both L257 and V94, yet is predicted to face outward rather than into the pocket. We reasoned that reducing the size of this side chain may provide additional space, modifying the width of the central cavity. According to the structural model, insertion of L256A and L257A residues partially expose the base of the cavity (Figure 5A). Fusion capacity of an F variant carrying these substitutions was reduced by approximately 50% as assessed by microscopic analysis (Figure 5A) and quantitative fusion assays (Figure 5B). Replacement of V94 by a larger methionine in the same mutant context (Table 1, no. 48), predicted to shield the base of the cavity, almost completely restored fusion capacity (Figure 5A,B), while insertion of a small alanine residue at position 94 in addition to L256A and L257A (Table 1, no. 49), suggested to completely expose the base

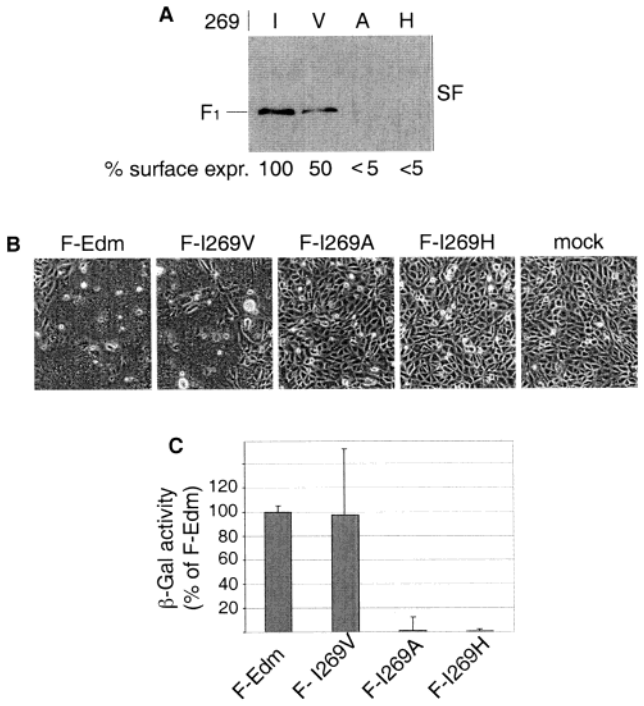

FIGURE 4: Hydrophobicity of residue 269 is important for F processing. (A) Cell surface expression; (B) syncytium induction; and (C) quantification of fusion activity for mutants F-I269V, F-I269A, and F-I269H were assessed as described in Figure 2A,C,D. Transfected Vero cells were photographed and analyzed 20 h post-transfection. Numbers (Figure 3A) indicate the relative percentage of F_1 detected in surface biotinylation in relation to F-Edm F_1 (% surface expression). In panel B, representative fields of view are shown.

of the cavity, abolished fusion activity (Figure 5A,B). Each of these changes was tolerated when made individually (Table 1, nos. 12, 15, and 3). While no change in steady-state level and hence stability of these mutants could be detected in Western analysis (data not shown), we observed a gradual reduction in cell surface expression that coincided with loss of fusion activity (Figure 5C). These results suggest that substitutions to smaller amino acids most likely interfere with folding and hence intracellular transport of the mutant molecules, but transport can be restored by insertion of a larger residue at the opposing wall of the cavity.

Transport-Competent Mutants with Widened Pockets Do Not Mediate Cell to Cell Fusion. That the progressive loss in fusion capacity of the mutants with gradually widened cavities coincided with their reduction in surface expression raises the question of whether widening the cavity solely interferes with intracellular transport or also with fusion activity (i.e., whether mutants with similarly opened pockets would be fusion competent if they would reach the cell surface). Two mutants identified in our screen provided evidence addressing this question, F-I225A L256A L257A and F-V94G L257A (Table 1, nos. 51 and 40). Both contained multiple substitutions to smaller amino acids that are predicted to render the base of the cavity partially solvent exposed (data not shown) but maintained transport competence, although to a reduced degree as compared to unmodified F-Edm (Figure 6A). Despite their transport competence, microscopic analysis of syncytia formation, quantification of fusion activity, and fluorescent lipid dye transfer revealed that these mutants were unable to induce fusion or hemifusion (Figure 6B,C). When analyzing F molecules harboring each of the individual substitutions present in these mutants independently, however, we observed that none of them greatly reduced fusion activity (Table 1, nos. 4, 11, 12, and 15). Thus, while mutations that are predicted to render the

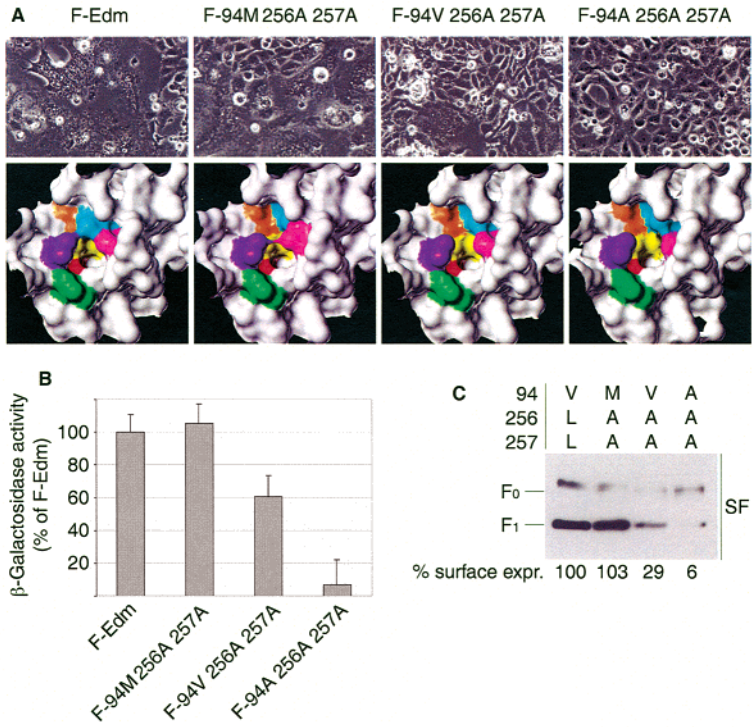

FIGURE 5: Small amino acid substitutions in the pocket that disrupt F processing can be compensated for by simultaneous insertion of larger residues. (A) Syncytium induction; (B) quantification of fusion activity; and (C) cell surface expression of mutants F-V94 L256A L257A, F-V94M L256A L257A, and F-V94A L256A L257A were assessed as described in Figure 2. Connolly type surface predictions were generated on the basis of energy-minimized derivatives of the MV F homology model. Coloring of residues corresponds to Figure 1C.

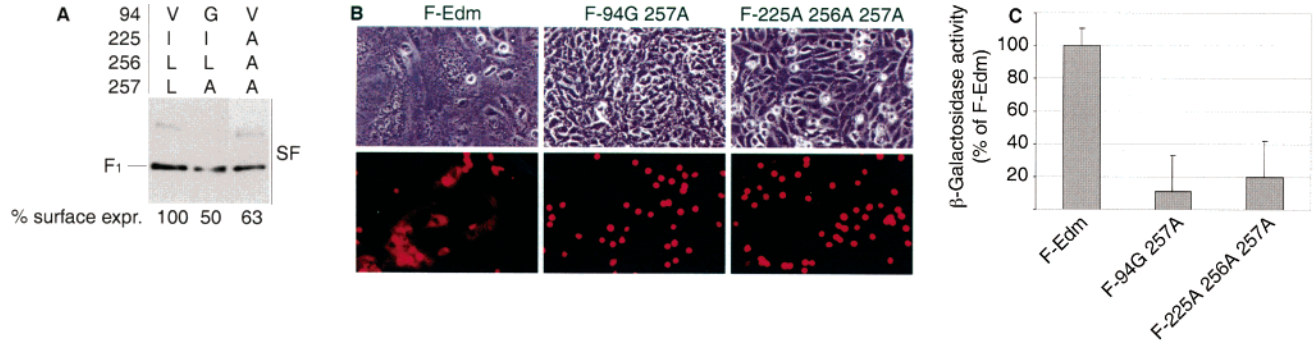

FIGURE 6: Transport-competent mutants with widened pockets do not induce syncytium formation. (A) Cell surface expression; (B) induction of syncytia and hemifusion; and (C) quantification of fusion activity of mutants F-I225A L256A L257A and F-V94G L257A. To assess hemifusion activity, Vero cells were transiently transfected with equal amounts of plasmid DNA encoding MV-H and F constructs as indicated and overlayed with R18 labeled red blood cells. Representative fields of view are shown. Surface expression and fusion activity were determined as described in Figure 2.

pocket more open can interfere with intracellular transport, they also result in loss of fusion competence of mutants that remain transport competent, suggesting a direct role for this F region in the fusion process as well as in F folding.

Insertion of Histidine Residues Results in a Reversible, pH-Dependent Arrest of Fusion. We found previously that inserting a charged asparagine residue at position 94 almost completely ablates fusion and hemifusion activity while not abolishing transport-competence (*27*). To explore whether the addition of charge, rather than an effect of residue size, is responsible for ablating fusion, we substituted several amino acids singly or in combination by histidine. Given a p*K* of 6.5, histidine is predicted to be charged at physiologic pH but may be neutralized at elevated pH, depending on the microenvironment. We hypothesized that these alterations might facilitate a reversible, pH-dependent arrest of fusion because of neutralization of charged histidine side chains at elevated pH. It might hence be possible to generate F mutants that are fusion inactive under physiologic conditions but become activated after a raise in pH.

When different histidine mutant constructs were coexpressed with MV-H, we found that fusion induced by F-T270H, F-V94H T270H, and F-L257H T270H (Table 1, nos. 26, 42, and 45) was almost completely inhibited under physiologic conditions, while at pH 8.5, at which histidine side chains may become deprotonated, fusion ranging from small, discrete syncytia to extensive giant cell formation was observed (Figure 7A). In contrast, fusion activity of the unmodified F-Edm protein was unaffected by these pH changes. Of the mutants analyzed, those carrying double substitutions at positions 270 and 94 or 257 were found to be most susceptible to activation by pH-dependent neutralization. Importantly, the ability of the activatable F variants to induce hemifusion at physiologic pH was likewise nearly completely abolished (Figure 7A) indicating that the charged histidine residues interfere with initial steps of the fusion process preceding lipid mixing. Quantification of fusion activity at pH 7.2 and 8.5 revealed a significant increase in reporter gene expression at elevated pH, confirming our microscopic observations (Figure 7B). However, F mutant L257H T270H (Table 1, no. 45) displayed an increased background activity at pH 7.2 that was not corroborated by visible syncytia formation or lipid dye transfer. This might be due to partial activation of this construct by detachment and manipulation of transfected cells prior to mixing with the target cell population. Nevertheless, this construct also showed a substantial increase in fusion activity upon pH shift to 8.5.

An advantage of this experimental approach is that the fusion capacity of each histidine mutant can be compared to the same mutant at different pH rather than to unmodified F-Edm, and incubation of cells at elevated pH is unlikely to alter protein stability and/or intracellular transport of the histidine containing mutant proteins. However, since this possibility could not be ruled out entirely, we determined their steady-state level and surface expression rate after incubation at pH 7.2 or 8.5. While the amount of total F protein and hence overall stability of the various constructs appeared similar to unmodified F-Edm (data not shown), we observed a significant reduction in intracellular transport, in particular of construct F-V94H T270H (Table 1, no. 42, Figure 7C). This finding was consistent with our previous observations that charged residues at position 94 reduce surface expression (*27*). Importantly however, the transport rate of all histidine constructs was not significantly influenced by the pH change, supporting the conclusion that neutralization of histidine residues accounts for the pH-dependent alterations in fusion activity.

DISCUSSION

We provide structural predictions and experimental evidence supporting the existence of a cavity that lies at the top of the MV F neck structure, directly beneath the trimeric globular head, and is important for both fusion and hemifusion. Sequence alignment reveals key features of this pocket to be conserved among distantly related paramyxoviruses, suggesting that it may function similarly in diverse members of this virus family.

We have previously identified amino acid 94 in the F_2 subunit of MV to be a determinant of viral fusogenicity (*27*). We also identified within MV F a potential third heptad repeat, HR-C, and localized amino acid 94 to the C-terminal half of this HR-C domain. Our previous finding that substitutions to small amino acids were tolerated at position 94, while changes to polar or charged residues disrupted either F processing or its fusion function, led us to suggest that amino acid 94 may mediate its effects on fusion via interaction with neighboring amino acids. To identify and study these interactions, we generated a homology model of the MV F protein based on the coordinates available for

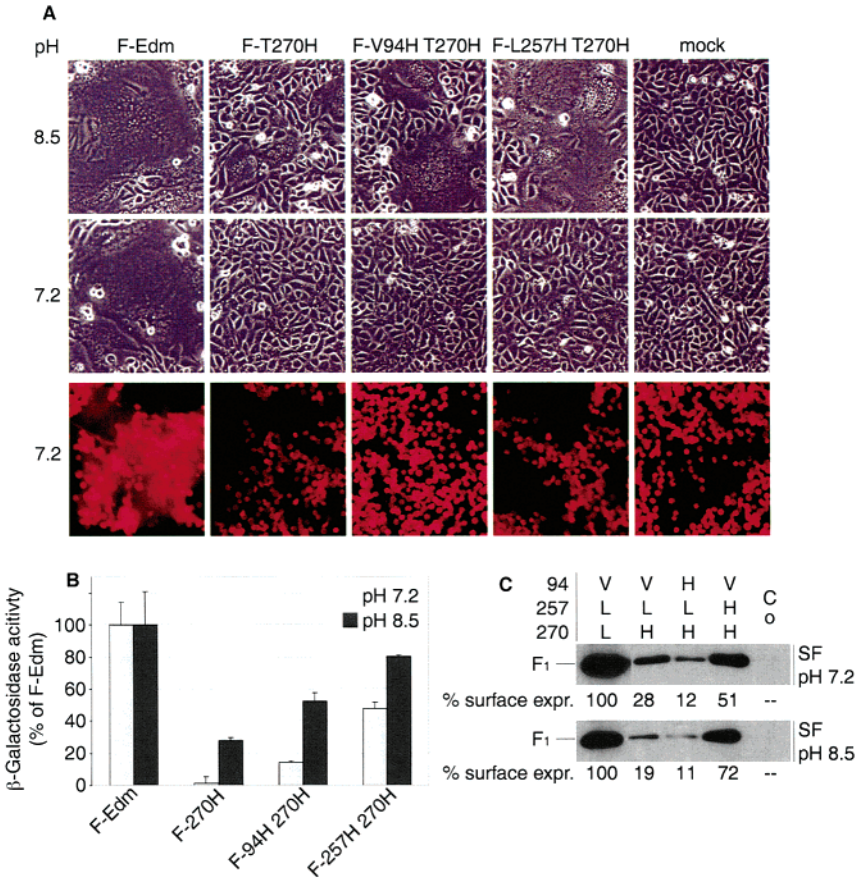

FIGURE 7: Insertion of histidine residues in the F pocket results in a reversible, pH-dependent arrest of fusion. (A) Syncytium formation and induction of hemifusion at pH 7.2 and 8.5; (B) quantification of fusion activity at pH 7.2 and 8.5; and (C) cell surface expression at pH 7.2 and 8.5 of mutants F-T270H, F-V94H T270H, and F-L257H T270H were determined as described in Figures 2 and 6B. Prior to analysis of syncytium formation, hemifusion, and F surface expression, Vero cells were incubated at different pH conditions for 20 h.

the NDV F protein. The model reveals the MV F HR-C region to be helical and to possess an outward kink in its C-terminal half, induced by the central proline of the conserved L/IXP motif. Amino acid 94 lies in this outwardly kinked region, in a defined cavity. Since the structural model guided our subsequent analyses, it was initially important to experimentally verify the basic features of the model around the HR-C domain. We found that the C-terminal HR-C regions of MV and NDV were functionally interchangeable, supporting our structure-based prediction that MV possesses a helical HR-C domain. Further support for the structural model came from our finding that loss of transport competence because of mutations to smaller residues can be compensated for by substitutions to larger residues at neighboring positions within the cavity. Also, hydrophobicity at the base of the predicted cavity was found to be essential for F folding, consistent with the propensity of hydrophobic residues to bury within the molecule in the vicinity of a hydrophilic environment.

The structural model predicts that the cavity is located at the top of the F neck, below the globular head of the trimer. We were able to derive a Connolly type surface model of the cavity, showing it to be comprised of a hydrophobic base and a partially hydrophilic rim, and our results indicate that both are important for F processing and transport. The location of the pocket within the trimer and our previous observation that amino acid 94 influences fusion (*27*) pointed to the pocket having a direct role in MV cell entry. This hypothesis was tested by a mutational analysis of the pocket. We found loss of function in mutants with predicted widened pockets to be due to both an indirect effect mediated through disruption of intracellular F transport and a direct effect on fusion itself. These data support the hypothesis that the F pocket is a direct mediator of F fusogenicity and suggest that the shape of the cavity may be able to modulate fusion efficiency.

The finding that substitution to a charged amino acid at residue 94 ablates fusion (*27*) suggests that the predominantly uncharged nature of the pocket may be important for its function. To further test this hypothesis, we introduced into the pocket several histidine residues, predicting that if a low degree of charge must be maintained for fusion to proceed, the additional charge present at physiologic pH should be inhibitory, while neutralizing these charges at pH 8.5 might enable fusion to proceed. Indeed, we identified several mutants that were activatable by elevated pH, inducing barely detectable cell-to-cell fusion at pH 7.2 and moderate to extensive syncytia formation at pH 8.5. Mutants carrying two histidine residues demonstrated the most marked pH-activation, inducing syncytia formation at pH 8.5 nearly as extensively as MV-Edm. These findings suggest that maintaining a low degree of charge in the F cavity environment is essential for MV entry to proceed.

Models of paramyxovirus cell entry differ in the trigger proposed to induce fusion, although most invoke receptor binding as the most likely fusion initiator, similar to the mechanism proposed for HIV-mediated fusion. Furthermore, it has been reported that conformational changes in H or

HN ensue (*39*). The end result is exposure of the F protein fusion peptide, formation of a stable six-helix core structure, and membrane merging. The steps intervening remain to be elucidated (*4*, *5*, *39*, *40*): conformational changes in H or HN conceivably trigger conformational changes in F that result in exposure of the fusion peptide, or facilitate binding of F to a second yet unidentified cellular receptor, and this interaction induces further changes in F that enable exposure of the fusion peptide. It was further proposed that the F globular heads shift or move apart to enable exposure of the fusion peptide (*12*, *13*). This rearrangement, although likely to ultimately affect most of the F trimer, conceivably requires a flexible domain in F that enables the initial outward movement of the globular head. Based on the location of the F pocket at a molecular surface at the top of the neck directly beneath the head of the F trimer, and our findings that residues in the F pocket directly influence fusion and that the degree of charge in the pocket is important for its function, we speculate that this region may form part of such a flexible domain.

Most models of paramyxovirus entry propose a similar mechanism for those family members that require both H (or HN or G) and F to mediate entry. Thus, some commonality of cell entry is likely between members of the Paramyxoviridae, suggesting that the F pocket may be a conserved feature of these viruses. Indeed, sequence analysis reveals key features of the F pocket to be conserved among distant members of the *Paramyxovirinae*, suggesting that the pocket may be present and may serve the same crucial function in other paramyxoviruses. The structurally constrained nature of the pocket renders it a potential target for the development of small molecule or peptide inhibitors that may fit into the cavity, thus inhibiting fusion. If the pocket is indeed a conserved feature of the paramyxovirus fusion machinery, it may constitute an attractive target for the rational design of antiviral agents active against diverse human and animal pathogens.

ACKNOWLEDGMENT

We thank M.A. Billeter for plasmids encoding the full-length MV-Edm genome, R. Cattaneo for plasmids encoding MV F, MV H, and antibodies directed against the MV F cytosolic tail, and A.L. Hammond for critical reading of the manuscript. Structural modeling was performed at the Biomolecular Computing Resource (BimCore) of Emory University.

REFERENCES

1. Lamb, R. A., and Kolakofsky, D. (1996) in *Fundamental Virology* (Howley, P. M., Ed.) pp 577−604, Lippencott-Raven, Philadelphia, PA.
2. WHO (2000) http://www.who.int/health-systems-performance/whr2000.htm.
3. Morrison, T. G., and Portner, A. (1991) in *The Paramxyoviruses* (Kingsbury, D. W., Ed.) pp 347−82, Plenum Press, New York.
4. Lamb, R. A. (1993) Paramyxovirus fusion: a hypothesis for changes, *Virology 197*, 1−11.
5. Dutch, R. E., Jardetzky, T. S., and Lamb, R. A. (2000) Virus membrane fusion proteins: biological machines that undergo a metamorphosis, *Biosci. Rep. 20*, 597−612.
6. Plemper, R. K., Hammond, A. L., and Cattaneo, R. (2001) Measles virus envelope glycoproteins hetero-oligomerize in the endoplasmic reticulum, *J. Biol. Chem. 276*, 44239−46.
7. Scheid, A., and Choppin, P. W. (1974) Identification of biological activities of paramyxovirus glycoproteins. Activation of cell fusion, hemolysis, and infectivity by proteolytic cleavage of an inactive precursor protein of Sendai virus, *Virology 57*, 475−90.
8. Homma, M., and Ouchi, M. (1973) Trypsin action on the growth of Sendai virus in tissue culture cells. 3. Structural difference of Sendai viruses grown in eggs and tissue culture cells, *J. Virol. 12*, 1457−65.
9. Carr, C. M., and Kim, P. S. (1993) A spring-loaded mechanism for the conformational change of influenza hemagglutinin, *Cell 73*, 823−32.
10. Chen, J., Lee, K. H., Steinhauer, D. A., Stevens, D. J., Skehel, J. J., and Wiley, D. C. (1998) Structure of the hemagglutinin precursor cleavage site, a determinant of influenza pathogenicity and the origin of the labile conformation, *Cell 95*, 409−17.
11. Wilson, I. A., Skehel, J. J., and Wiley, D. C. (1981) Structure of the haemagglutinin membrane glycoprotein of influenza virus at 3 Å resolution, *Nature 289*, 366−73.
12. Chen, L., Gorman, J. J., McKimm-Breschkin, J., Lawrence, L. J., Tulloch, P. A., Smith, B. J., Colman, P. M., and Lawrence, M. C. (2001) The structure of the fusion glycoprotein of Newcastle disease virus suggests a novel paradigm for the molecular mechanism of membrane fusion, *Structure 9*, 255−66.
13. Peisajovich, S. G., and Shai, Y. (2002) New insights into the mechanism of virus-induced membrane fusion, *Trends. Biochem. Sci. 27*, 183−90.
14. Bullough, P. A., Hughson, F. M., Skehel, J. J., and Wiley, D. C. (1994) Structure of influenza haemagglutinin at the pH of membrane fusion, *Nature 371*, 37−43.
15. Chan, D. C., Fass, D., Berger, J. M., and Kim, P. S. (1997) Core structure of gp41 from the HIV envelope glycoprotein, *Cell 89*, 263−73.
16. Weissenhorn, W., Dessen, A., Harrison, S. C., Skehel, J. J., and Wiley, D. C. (1997) Atomic structure of the ectodomain from HIV-1 gp41, *Nature 387*, 426−30.
17. Caffrey, M., Cai, M., Kaufman, J., Stahl, S. J., Wingfield, P. T., Covell, D. G., Gronenborn, A. M., and Clore, G. M. (1998) Three-dimensional solution structure of the 44 kDa ectodomain of SIV gp41, *EMBO J. 17*, 4572−84.
18. Kobe, B., Center, R. J., Kemp, B. E., and Poumbourios, P. (1999) Crystal structure of human T cell leukemia virus type 1 gp21 ectodomain crystallized as a maltose-binding protein chimera reveals structural evolution of retroviral transmembrane proteins, *Proc. Natl. Acad. Sci. U.S.A. 96*, 4319−24.
19. Fass, D., Harrison, S. C., and Kim, P. S. (1996) Retrovirus envelope domain at 1.7 Å resolution, *Nat. Struct. Biol. 3*, 465−9.
20. Weissenhorn, W., Carfi, A., Lee, K. H., Skehel, J. J., and Wiley, D. C. (1998) Crystal structure of the Ebola virus membrane fusion subunit, GP2, from the envelope glycoprotein ectodomain, *Mol. Cell 2*, 605−16.
21. Matthews, J. M., Young, T. F., Tucker, S. P., and Mackay, J. P. (2000) The core of the respiratory syncytial virus fusion protein is a trimeric coiled coil, *J. Virol. 74*, 5911−20.
22. Baker, K. A., Dutch, R. E., Lamb, R. A., and Jardetzky, T. S. (1999) Structural basis for paramyxovirus-mediated membrane fusion, *Mol. Cell 3*, 309−19.
23. Yu, M., Wang, E., Liu, Y., Cao, D., Jin, N., Zhang, C. W., Bartlam, M., Rao, Z., Tien, P., and Gao, G. F. (2002) Six-helix bundle assembly and characterization of heptad repeat regions from the F protein of Newcastle disease virus, *J. Gen. Virol. 83*, 623−9.
24. Skehel, J. J., and Wiley, D. C. (1998) Coiled coils in both intracellular vesicle and viral membrane fusion, *Cell 95*, 871−4.
25. Lambert, D. M., Barney, S., Lambert, A. L., Guthrie, K., Medinas, R., Davis, D. E., Bucy, T., Erickson, J., Merutka, G., and Petteway, S. R., Jr. (1996) Peptides from conserved regions of paramyxovirus fusion (F) proteins are potent inhibitors of viral fusion, *Proc. Natl. Acad. Sci. U.S.A. 93*, 2186−91.
26. Smith, B. J., Lawrence, M. C., and Colman, P. M. (2002) Modelling the structure of the fusion protein from human respiratory syncytial virus, *Protein Eng. 15*, 365−71.
27. Plemper, R. K., and Compans, R. W. (2003) Mutations in the putative HR-C region of the measles virus F2 glycoprotein modulate syncytium formation, *J. Virol. 77*, 4181−90.
28. Radecke, F., Spielhofer, P., Schneider, H., Kaelin, K., Huber, M., Dotsch, C., Christiansen, G., and Billeter, M. A. (1995) Rescue of measles viruses from cloned DNA, *EMBO J. 14*, 5773−84.

29. Thompson, J. D., Higgins, D. G., and Gibson, T. J. (1994) CLUSTAL W: improving the sensitivity of progressive multiple sequence alignment through sequence weighting, position-specific gap penalties, and weight matrix choice, *Nucleic Acids. Res. 22*, 4673−80.
30. Sali, A., and Blundell, T. L. (1993) Comparative protein modelling by satisfaction of spatial restraints, *J. Mol. Biol. 234*, 779−815.
31. Yriend, G. (1990) WHAT IF: A molecular modeling and drug design program, *J. Mol. Graph. 8*, 52−6.
32. Cathomen, T., Buchholz, C. J., Spielhofer, P., and Cattaneo, R. (1995) Preferential initiation at the second AUG of the measles virus F mRNA: a role for the long untranslated region, *Virology 214*, 628−32.
33. Singh, M., Cattaneo, R., and Billeter, M. A. (1999) A recombinant measles virus expressing hepatitis B virus surface antigen induces humoral immune responses in genetically modified mice, *J. Virol. 73*, 4823−8.
34. Calain, P., and Roux, L. (1993) The rule of six, a basic feature for efficient replication of Sendai virus defective interfering RNA, *J. Virol. 67*, 4822−30.
35. Plemper, R. K., Hammond, A. L., and Cattaneo, R. (2000) Characterization of a region of the measles virus hemagglutinin sufficient for its dimerization, *J. Virol. 74*, 6485−93.
36. McGinnes, L. W., and Morrison, T. G. (1986) Nucleotide sequence of the gene encoding the Newcastle disease virus fusion protein and comparisons of paramyxovirus fusion protein sequences, *Virus Res. 5*, 343−56.
37. Bukau, B., and Horwich, A. L. (1998) The Hsp70 and Hsp60 chaperone machines, *Cell 92*, 351−66.
38. Ellgaard, L., Molinari, M., and Helenius, A. (1999) Setting the standards: quality control in the secretory pathway, *Science 286*, 1882−8.
39. Takimoto, T., Taylor, G. L., Connaris, H. C., Crennell, S. J., and Portner, A. (2002) Role of the hemagglutinin-neuraminidase protein in the mechanism of paramyxovirus-cell membrane fusion, *J. Virol. 76*, 13028−33.
40. McGinnes, L. W., Gravel, K., and Morrison, T. G. (2002) Newcastle disease virus HN protein alters the conformation of the F protein at cell surfaces, *J. Virol. 76*, 12622−33.

BI034385K